Water Resources Research

RESEARCH ARTICLE
10.1029/2019WR026611

Constraining the Assimilation of SWOT Observations With Hydraulic Geometry Relations

K. M. Andreadis[1], **C. B. Brinkerhoff**[1], **and C. J. Gleason**[1]

[1]Department of Civil and Environmental Engineering, University of Massachusetts, Amherst, MA, USA

Key Points:
- Data assimilation of SWOT observations can retrieve large-river discharge even with a simple steady-state model
- A data-driven approach led to a plausible estimation of prior probability distributions of hydraulic variables
- Hydraulic geometry constraints improved river discharge estimation accuracy across all metrics

Supporting Information:
- Supporting Information S1

Correspondence to:
K. M. Andreadis,
kandread@umass.edu

Citation:
Andreadis, K. M., Brinkerhoff, C. B., & Gleason, C. J. (2020). Constraining the assimilation of SWOT observations with hydraulic geometry relations. *Water Resources Research*, *56*, e2019WR026611. https://doi.org/10.1029/2019WR026611

Received 23 OCT 2019
Accepted 30 APR 2020
Accepted article online 12 MAY 2020

Abstract The Surface Water Ocean Topography (SWOT) satellite mission expected to launch in 2021 will offer a unique opportunity to map river discharge at an unprecedented spatial resolution globally from observations of water surface elevation, width, and slope. Because river discharge will not be directly observed from SWOT, a number of algorithms of varying complexity have been developed to estimate discharge from SWOT observables. Outstanding issues include the lack of accurate prior information and parameter equifinality. We developed a new data assimilation discharge algorithm that aimed to overcome these limitations by integrating a data-driven approach to estimate priors with a model informed by hydraulic geometry relations. A comprehensive simulated dataset of 18 rivers was used to evaluate the algorithm and four different configurations (rectangular channel, generic channel, and geomorphologically classified channel with and without regularization) to assess the impact of progressively adding hydraulic geometry constraints to the estimation problem. The algorithm with the full set of constraints outperformed the other configurations with median Nash-Sutcliffe coefficients of 0.77, compared with −0.46, 0.31 and 0.66, while other error metrics showed similar improvement. Results from this study show the promise of this hybrid data-driven approach to estimating river discharge from SWOT observations, although a number of enhancements need to be tested to improve the operational applicability of the algorithm.

1. Introduction

Water is essential for all ecosystems and civilizations and better understanding of global hydrology benefits numerous fields of study. Currently, the best available tool to understand the water cycle at any place on earth is a gauging station, where in situ instruments record water level and convert this quantity to mass flux/discharge via empirically calibrated functions (i.e., rating curves). These gauges are well understood and accurate when properly maintained, but gauge maintenance requires physical site access at considerable expense. Gauges are therefore declining worldwide as they are defunded or as sharing their information becomes too politically sensitive (Gleason & Hamdan, 2017; Hannah et al., 2011). The loss of these primary observations impairs our ability to tune land surface models, which in turn affects our understanding of the impacts of climate change, our ability to manage scarce water resources, and our general knowledge of the state of the global hydrosphere. Since all models are primarily a function of the quality of their input data, additional primary information is needed to augment gauges and improve hydrologic understanding worldwide.

Remote sensing is gaining attention as a valuable tool for hydrologists attempting to fill the temporal and spatial gaps in global observation networks (McCabe et al., 2017). Early work built on the legacy of gauges, using satellite observations of width or water surface elevation in a similar manner as a traditional gauge, and this work has continued to the present day (e.g., Ashmore & Sauks, 2006; Pavelsky, 2014; Smith & Pavelsky, 2008). Moreover, rating curves could also be built from observations of other quantities from space (as opposed to width/water surface elevation), and this work also is ongoing (e.g., Bjerklie et al., 2018; Dijk et al., 2016; Tarpanelli et al., 2013). Both of these approaches rely on some in situ data to develop empirical equations for discharge and are successful in doing so. However, in truly ungauged regions, training data must come from outside the basin and thus invoke assumptions of hydrologic transferability that could be problematic (e.g., Coron et al., 2012).

To address this need in ungauged basins and supplement existing in situ networks with synoptic measurements, NASA/CNES/CSA/UKSA have been developing the Surface Water and Ocean Topography (SWOT)

mission, designed to provide simultaneous observations of water surface elevation (WSE), width, and slope on all global rivers wider than 100 m (Biancamaria et al., 2016). SWOT would also allow for indirect observations of river discharge globally, covering more than 60% of 50,000 km^2 basins with 100 m rivers. In contrast, current in situ capabilities (from freely available datasets) correspond to 30% of basins with 100 m rivers (Pavelsky et al., 2014). Moreover, recent studies have demonstrated potential approaches to estimating discharge in smaller rivers than those directly observed from SWOT by transferring information upstream (e.g., Paiva et al., 2015). Many methods designed for estimating river discharge from SWOT operate under the same basic principle, the so-called Mass conserved Flow Law Inversion (McFLI) (Gleason et al., 2017). This approach allows discharge estimation in the absence of any in situ data or transferability assumptions and attempts to solve an underconstrained optimization problem for the discharge needed to produce the hydraulic conditions observed via remote sensing. A number of algorithms have been developed that can be considered to follow the mass-conserved flow inversion approach and range in complexity from Markov chain Monte Carlo (Durand et al., 2014), Hamiltonian Monte Carlo (Hagemann et al., 2017), and variational and Kalman Filter data assimilation schemes (Andreadis et al., 2007; Biancamaria et al., 2011; Oubanas, Gejadze, Malaterre & Mercier, 2018). This approach has also been successfully deployed using optical satellite observations (Feng et al., 2019; Gleason et al., 2018), but SWOT's synoptic observations should provide the most accurate discharge estimates with acceptable accuracy for numerous river types (Pavelsky et al., 2014), including complex cases such as estuaries (e.g., Chevalier et al., 2019) and braided rivers (e.g., Garambois et al., 2017).

Previous SWOT-based McFLI approaches have shown great promise, but their implementation and evaluation have revealed some issues that could hinder their accuracy and applicability. First, SWOT-based data assimilation schemes require a hydraulic model to provide predictions of discharge that can then be inverted when combined with the SWOT observations. However, these models have tended to be rather complex and have either significant data requirements or prodigious computational expense. Furthermore, even the algorithms that do not require a complex hydraulic model benefit from prior information (e.g., discharge or river bathymetry) and when such a priori knowledge is not accurate or is unavailable, the algorithm's performance is compromised (Bonnema et al., 2016). Another issue that afflicts such estimation algorithms is equifinality, which refers to the existence of multiple sets of variables (discharge, bed elevation, roughness, etc.) that can lead to the same flow profile as the one observed and thus makes the estimation problem ill-posed (Garambois & Monnier, 2015).

One way to ameliorate the equifinality issue is to introduce additional constraints to the optimal estimation problem. At-a-station hydraulic geometry (AHG) theory has been confirmed both empirically and theoretically (Gleason, 2015) and can be independent from the Manning's equation on which most of the aforementioned algorithms are based (Durand et al., 2016). Essentially, AHG emerged from observing that river flow width, depth, and velocity vary linearly (in log-space) with discharge for a specific river cross section. Ferguson (1986) first confirmed that these power laws are directly linked to common channel geometric form, and Dingman (2007) proposed a simple mathematical model for channel geometry that reliably yields AHG. These relationships can be incorporated into the estimation scheme of a SWOT discharge algorithm to reduce the viable parameter space for the mass-conserved flow inversion.

We developed a data assimilation algorithm, the SWOT Assimilated Discharge (SAD), that utilizes a simplified hydraulic scheme to estimate river discharge from SWOT satellite observations. In contrast to other data assimilation techniques that have demonstrated the retrieval of discharge from SWOT-like observations, SAD uses a hydraulic model with minimal data requirements, making it well-suited for application globally, and uses a data-driven approach to derive prior probability distributions for the algorithm's input parameters. We assessed the performance of the algorithm within the context of synthetic SWOT observations by sequentially incorporating hydraulic geometry relations into the estimation of river discharge.

2. Algorithm Description

The SAD algorithm operates on the set of SWOT observables (i.e., WSE, width, and slope) and derives an estimate of river discharge and its associated uncertainty using a data assimilation scheme. The assimilation scheme involves the "first-guess" estimation of hydraulic variables by combining a forward model with a set of prior probability distributions before assimilating the SWOT observations. The priors are estimated with a sampling approach, as these data-driven methods have shown promise in many fields (e.g., Ichii et al., 2017).

The objective of the algorithm is to estimate discharge at each river reach when SWOT observations become available.

2.1. Hydraulic Model

The forward model in the assimilation scheme is based on the Gradually Varied Flow (GVF) equations, which describe the steady-state, non-uniform flow in river channels with gradual variations in water depth and velocity. The general form of the GVF equation (Chow, 1955) is

$$\frac{dY}{dx} = \frac{S_0 - S_f}{1 - Fr^2} \tag{1}$$

where Y is the average water depth, x is the longitudinal distance, S_0 is the channel bed slope, S_f is the water surface slope, and Fr is the Froude number. The latter is given by

$$Fr = \frac{Q}{WY\sqrt{gY}} \tag{2}$$

where W is the average flow width, Q is river discharge, and g is the gravity acceleration, while the water surface slope can be calculated as a function of discharge, channel geometry, and flow resistance. The specification of flow resistance (or its inverse, conductance) is not straightforward, as it varies with flow and boundary conditions (Leopold et al., 1960). Here, we opted to specify S_f from the Manning equation (see supporting information Text S1 for details), which is the most widely used approach to characterizing reach-scale flow resistance (Ferguson, 2013). It is well documented that the Manning equation cannot capture the full complexity of river flows, especially considering the fixed (and global) exponent on the velocity-depth relation and the assumption of stage-invariant flow resistance (Bjerklie et al., 2005; Ferguson, 2010; Katul et al., 2002; Wang et al., 2019). Nonetheless, this arithmetically simple formulation allows for computational efficiency and maximum flexibility and for large rivers in particular Manning's equation is often invoked without great loss of discharge accuracy. Further, the formulation of the GVF model allows for the use of alternative flow resistance equations that could potentially be used in future versions of the SAD algorithm.

Integrating the GVF equations allows for calculation of longitudinal profiles of water surface elevation along a river. Equation (1) can be solved using a Runge-Kutta method (Rackauckas & Nie, 2017) for each satellite overpass of a river and used to generate a water surface elevation profile given characteristics of the river channel geometry, roughness coefficient, and river discharge (observed or from a prior estimate). To incorporate AHG theory into the model, channel cross sections are modeled following Dingman (2007) with a form that facilitates the association of SWOT observables and hydraulic geometry coefficients.

Figure 1 shows a schematic of the cross section geometry, where W^*, W, Y_m^*, Y_m are the bankfull width, water surface width, bankfull maximum depth, and maximum depth respectively. The latter are related to the average width and flow depth via a channel shape parameter r:

$$Y = \left(\frac{r}{r+1}\right) Y_m \tag{3}$$

$$W = W^* \left(\frac{Y_m}{Y_m^*}\right)^{1/r} \tag{4}$$

Hydraulic geometry relations can be incorporated into the SAD GVF model through the relationships between the AHG coefficients and exponents and the channel cross-section geometric variables:

$$W = aQ^b \tag{5}$$

$$Y = cQ^f \tag{6}$$

$$U = kQ^m \tag{7}$$

These relationships can be rewritten to relate the AHG coefficients and exponents with river channel geometry variables such as bankfull width and maximum depth, the channel shape parameter r, and the

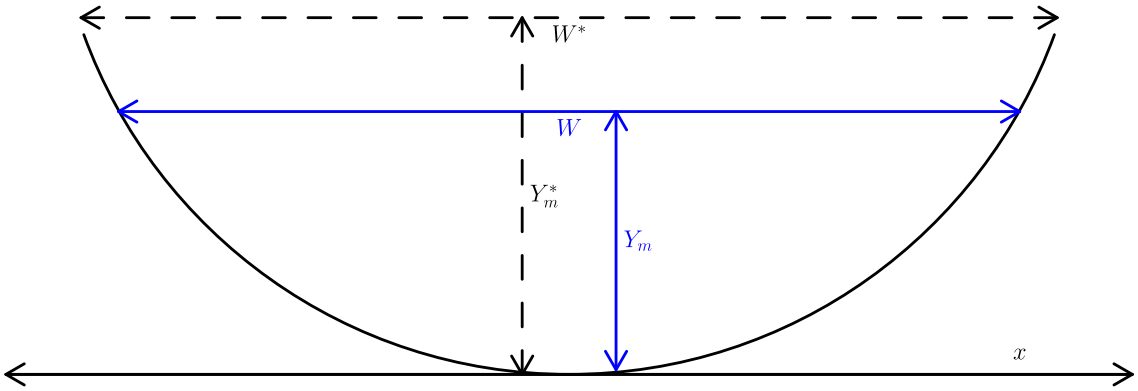

Figure 1. Simplified schematic of river channel cross-section geometry (adapted from Dingman, 2007).

friction slope (see Dingman and Afshari, 2018, and Text S2 in the supporting information for details). The r parameter ($0 < r < \infty$) reflects the river channel shape, with $r = 1$ corresponding to a triangular channel. As r increases, the channel banks become steeper, and the bottom becomes flatter leading to a rectangular channel for $r \to \infty$. There are various methods to estimate r from channel geometry or other measurements (Moramarco et al., 2019) as well as from the AHG coefficients (if they can be calculated independently), but here we treat r as a stochastic variable with an associated probability distribution.

2.2. Data Assimilation Scheme

The assimilation algorithm employed in the implementation of SAD presented here is the Local Ensemble Transform Kalman Filter (LETKF) (Hunt et al., 2007). The LETKF is a variant of the Ensemble Kalman Filter (Evensen, 2003) that combines a prior probability distribution of state variables (e.g., river discharge) with direct or indirect observations (in this case, water surface elevation and width) to generate an optimal estimate (i.e., analysis). The prior distribution is represented by the model error covariance, which is calculated empirically from an ensemble of unknown model states (i.e., background ensemble). The observations and their uncertainty are represented by mapping the state variables to the observations space (e.g., river discharge to water surface elevation) and an error covariance. The analysis state (both the mean and the ensemble deviations from the mean) is essentially calculated as a function of the prior model ensemble, the model and observation error covariances, and the difference between the model-predicted observations and the actual observations (the details of the LETKF are given in supporting information Text S3). The LETKF explicitly supports localization by applying the analysis equations for local patches of the model domain using a subset of observations for each. In the case of the SAD algorithm, the model domain consists of a river network partitioned into reaches with each reach partitioned into cross sections. Therefore, the state vector is formed with river discharge at each river reach, while the truncated (i.e., local) observation vector consists of the nearest observations in terms of along-channel flow distance (García-Pintado et al., 2015). The observation vector consists of the SWOT observations at the cross section locations, and although the default variable in this study was water surface elevation, it can optionally include width and slope as well.

The estimation of river discharge from future SWOT observations can be difficult when bed elevation and/or roughness are unknown due to equifinality (Oubanas, Gejadze, Malaterre, Durand, et al., 2018). One approach that can aid in the solution of such problems is regularization (e.g., Budd et al., 2011), wherein additional constraints are introduced in the form of penalty terms similar to the observation difference applied to the LETKF analysis calculation. In the case of river discharge estimation, additional constraints can be derived from the at-a-station hydraulic geometry relations (equations (5)–(7)). In particular, it can be shown that assimilating "observations" of the form $W - aQ^b = 0$, for example, is equivalent to a form of regularization (Johns & Mandel, 2008) that is adding prior knowledge (in our case adherence to the AHG equations) to help solve an ill-posed inverse problem, before assimilating the actual observations.

2.3. Derivation of Priors

Ensemble assimilation methods require the definition of a prior probability distribution from which to generate the ensemble of background variables (Evensen, 2004). Given that our discharge estimation approach needs to be applicable globally, the algorithm must operate on the assumption of minimal prior knowledge

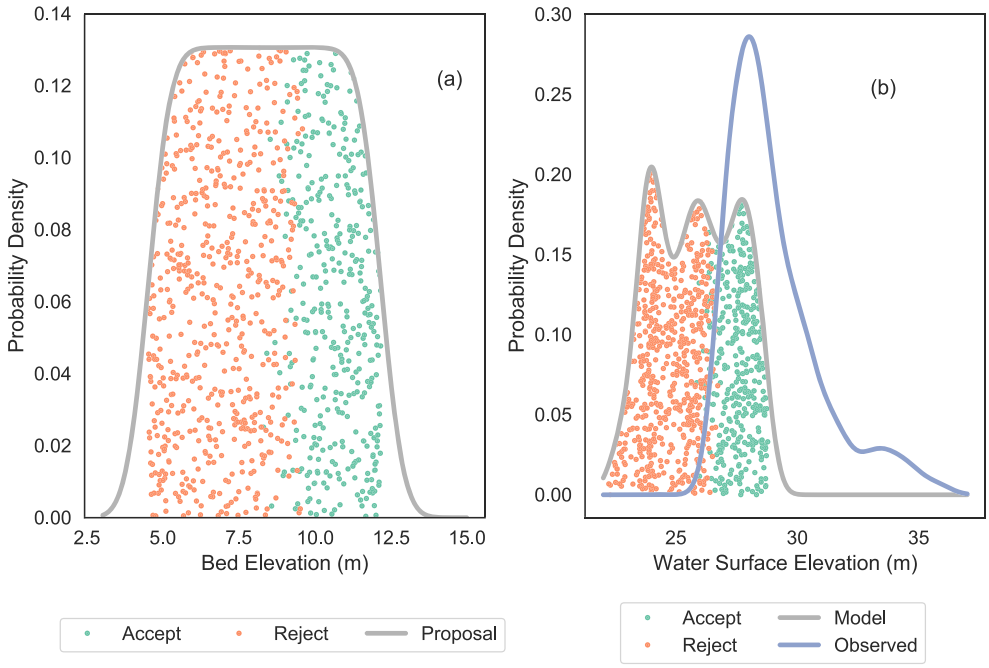

Figure 2. (a) Proposal PDF for downstream bed elevation and sampled points (showing both the subsequently rejected and accepted). (b) Estimated PDF (Model) from stochastic model simulation of upstream water surface elevation with bed elevation sampled from proposal PDF. Accepted/rejected water surface elevation points did/did not fall under the PDF derived from observations (Observed), with each point corresponding to a bed elevation sample.

regarding river discharge and the various inputs to the GVF model. Therefore, the algorithm starts with uninformative priors but uses the observations in a data-driven approach to estimate the necessary prior probability distributions. The inputs to the GVF model that are not directly observed include discharge, bed elevation (as well as bed slope), the roughness coefficient, and the channel shape parameter r.

We adapted a rejection sampling approach to derive appropriate prior distributions for these variables. Rejection sampling is a technique used to generate samples from the target distribution T using the proposal distribution P. Instead of directly sampling from T, the method generates samples from P and accepts/rejects each of those samples according to likelihood ratio

$$\frac{t(x)}{Lp(x)} \tag{8}$$

where L is a constant ($L > 1$) and $t(x), p(x)$ are the density functions of T and P, respectively (Martino et al., 2018). In our case, the target distribution is the prior distribution of the unobserved variable (e.g., bed elevation) and the proposal distribution is an uninformative prior. Since the density function of the target distribution is unknown, we use the GVF model as a functional to transform both densities $t(x)$ and $p(x)$ to correspond to density functions of water surface elevation instead of the target variable. The probability density function of WSE can be estimated from the observations, thus allowing us to calculate the likelihood ratio and accept/reject the proposed target-variable value for its prior distribution.

Figure 2 shows an example of the rejection sampling approach for estimating the prior distribution of bed elevation. The algorithm starts with an uninformative prior as the proposal distribution, from which a set of bed elevation values are sampled (Figure 2a). The uninformative priors are set as uniform distributions with the bounds for each unobserved variable described in Table 1. Each of the sampled bed elevation values are used as inputs to the GVF model to simulate an ensemble of WSE values, with each value in that ensemble corresponding to a bed elevation value. Using kernel density estimators for the PDFs of the observed and model WSE, the likelihood ratio defined above (equation (8)) can be calculated and each ensemble value pair can be accepted or rejected (Figure 2b). Subsequently, a new distribution can be calculated from the accepted samples of bed elevation, forming the prior to be used in the assimilation.

Table 1
Distribution Type and Parameters for the Uninformative Priors Used in the Rejection Sampling Approach

Variable	Distribution	Parameters
Bed elevation (z)	Uniform	$[H_{min}^{swot} - 20, H_{min}^{swot}]$
Discharge (Q)	Uniform	$[Q_{mean}/10, Q_{mean} * 10]$
Roughness (n)	Uniform	[0.01, 0.07]
Shape parameter r	Estimated	See section 3

Commonly used rejection sampling methods may suffer from low acceptability rates, making them inefficient when used to estimate posterior distributions (Vrugt & Beven, 2018). In the case of the SAD algorithm, we use such methods to identify the prior distribution where the parameter space can be relatively large as long as it contains behavioral solutions (i.e., solutions with non-zero likelihood; Blasone et al., 2008) for the particular river. Moreover, the GVF model is simple enough to make the generation of large populations to sample from computationally efficient. Following previous studies that evaluated the performance of SWOT discharge algorithms, we chose to only use a mean annual flow (Q_{mean}) estimated from a global water balance model as a prior estimation of mean flow (Durand et al., 2016) for the purposes of consistency. In cases where additional information on river discharge or bed elevation is available, it can be used to improve the performance of the SAD algorithm.

3. Geomorphological Classification

The at-a-station hydraulic geometry relations that were implicitly incorporated into the GVF model via the derivations of Dingman (2007) depend on the specification of the shape parameter r. In the absence of simultaneous data on discharge and width/depth, the estimation of r becomes difficult and therefore must be treated stochastically within the SAD assimilation algorithm. Nonetheless, an approach that constrains the probable values of r for each river would theoretically improve the accuracy of discharge estimation.

We developed a two-tiered approach to constrain the r parameter, with the first step a global predictive model for r using SWOT-observable variables as predictors and the second step a supervised expert classification framework based on river planform geometry. Both the estimation and classification were trained on empirically derived r values from HYDRoSWOT (Canova et al., 2016), a collection of over 200,000 USGS field hydraulic measurements (originally made for calibrating rating curves for USGS gages) across the continental United States and Alaska. Observed r values equate to f/b, where f and b are the exponents of the depth and width at-a-station hydraulic geometry relationships, respectively, fit at each cross section. Stations with physically impossible AHG results, such as $f < 0$ or $f > 1$ were excluded, as were stations with less than 20 measurements, leaving 479 stations and 14,402 measurements to train and test the classification.

The unsupervised predictive model uses a random forest algorithm to predict r values from variables that can be derived directly from SWOT observations such as river width and water surface elevations. A large number (500) of random regression trees were run, with one variable randomly sampled at each split. Using HYDRoSWOT data, WSE was defined as the sum of mean depth and datum height at-a-station, and bankfull width was defined as a given station's 75th percentile of width measurements. This model explains 96% of variance in the dataset's r values and was successfully validated on an independent set of the data ($R^2 = 0.98$, RMSE = 0.23). The accuracy of the model is partly dependent on the estimated bankfull width, and therefore, the validity of the 75th percentile assumption, as well as the assumption that SWOT observations capture high-flow conditions, would affect the results of the classification. Note that the model predicts a range of r values at-a-station, despite our definition of r as constant at-a-station. This is a consequence of having a time series of predictor variables (e.g., width and depth) yet a single r at each station, but in the case of the SAD algorithm, it allows us to construct distributions of potential r mean values for a given cross section.

The supervised expert classification scheme relies on assessing river planform geometry and making an informed decision of reach geomorphology (Figure 3). First, r was conceptually mapped onto classic river classification frameworks (Church, 2006; Rosgen, 1994; Schumm, 1985). Given the definition of r, highly stable and meandering to straight rivers should exhibit large r values, while unstable and frequently avulsing multi-threaded systems will exhibit low r values as they move more rapidly in the vertical direction

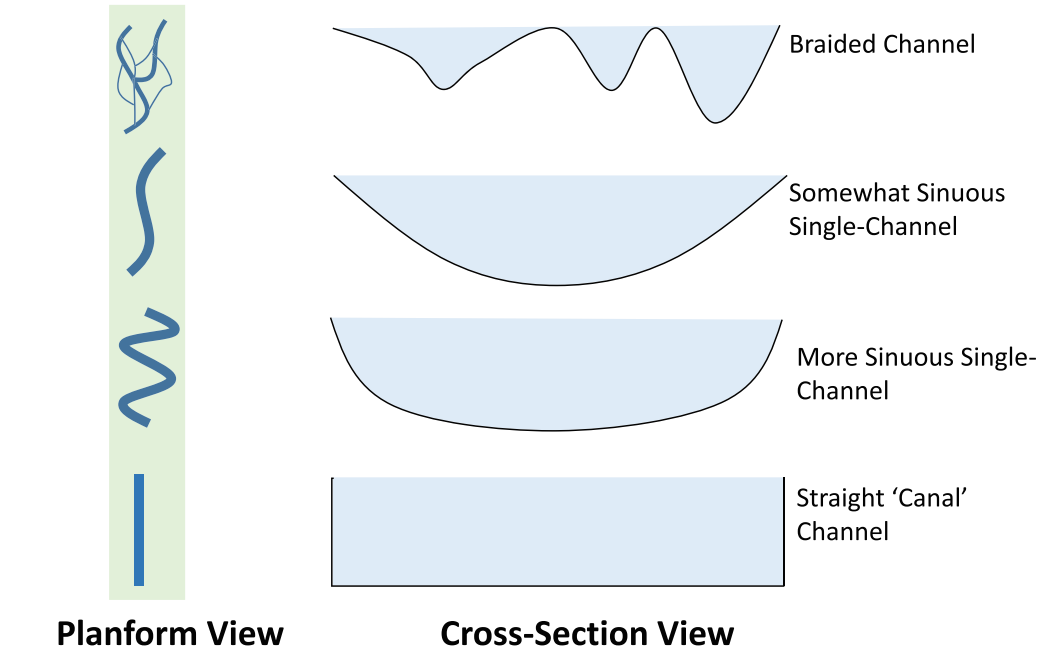

Figure 3. Classes of river planform geometry defined by the expert classification algorithm.

than in a horizontal plane as a meandering channel would. HYDRoSWOT empirical r values were qualitatively assessed to determine class thresholds. We noted that sinuous single channels generally had r values between 1 and 10, straight "canal"-like channels had values over 10, and r values below 1 resembled both braided channels and wide, shallow channels near dams (verified visually in Google Earth). We further decided that for the purposes of this algorithm, r values below 1 would correspond only to braided reaches. We are aware of the plethora of multi-channel river types, and in particular the differences between stable anastomosed channels and constantly shifting braided rivers, yet to maintain the nomenclature of Durand et al. (2016) for later comparison, these multi-threaded systems are simply referred to as braided. Class thresholds were finally set according to these observations and then compared against the frequency distribution of HYDRoSWOT r values as a qualitative check. The expert framework's class bounds approximate the following bins: 0–50th percentile ($r < 1$), 50–75th percentile ($1 < r < 5$), 75th to outlier threshold ($5 < r < 10$), and the outliers ($r > 10$). Within SAD, the bounds for each river class were used to truncate the probability distribution of the r parameter, with the mean and variance of that distribution (assumed to be Gaussian) derived from the unsupervised predictive model. Table 2 shows the class of each river from the 18 case studies using the geomorphological classification framework, along with the bounds for the r parameter for each class.

Table 2
Classification of Each River From the 18 Case Studies Using the Geomorphological Framework

Classification	Rivers	
Braided	Ganges, Platte, Tanana	r < 1
Somewhat Sinuous Single-Channel Reach	GaronneDownstream, GaronneUpstream, Kanawha, MississippiDownstream, Ohio, Po, SacramentoUpstream, Severn	1 < r < 5
More Sinuous Single-Channel Reach	Cumberland, MississippiUpstream, SacramentoDownstream, Seine, Wabash	5 < r < 10
Straight/Canal Reach	StLawrenceDownstream, StLawrenceUpstream	r > 10

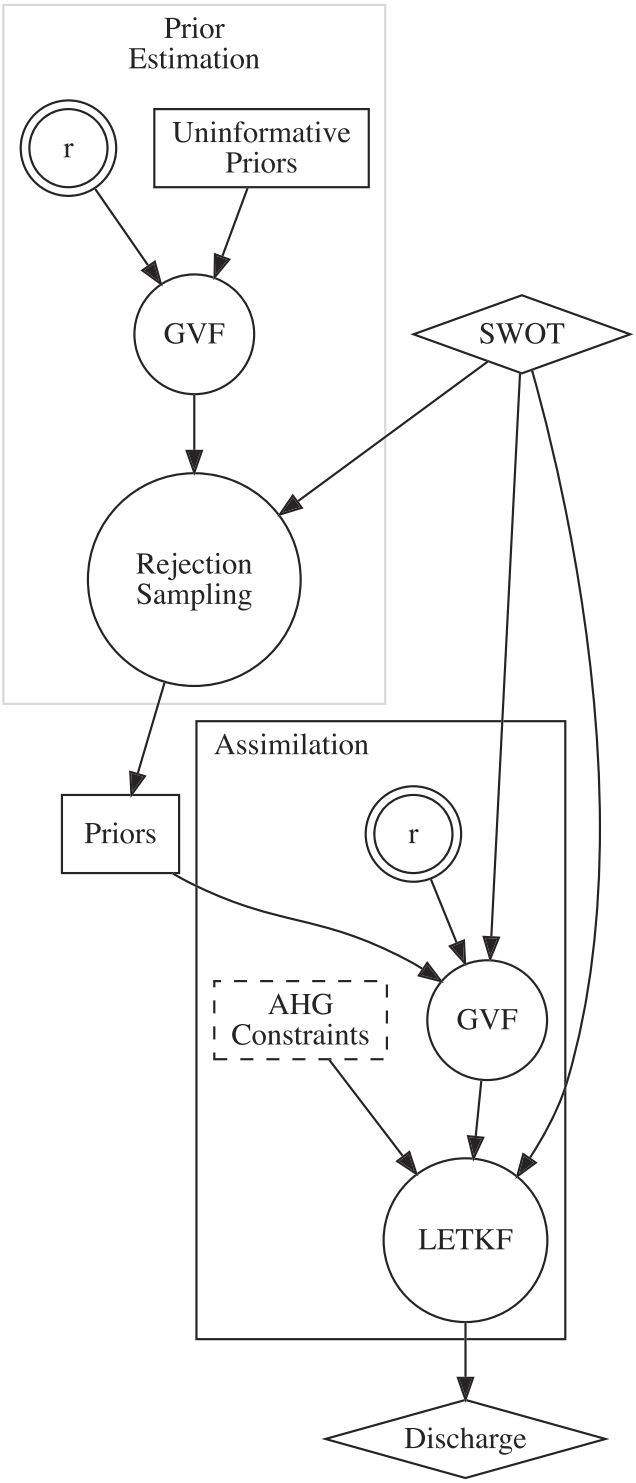

Figure 4. Flow diagram describing the SAD algorithm and the procedure for specifying the configurations for the experimental design (via the parameter *r*).

Table 3
Equations Describing Each of the Error Metrics Used to Evaluate the SAD Algorithm, With Q and $\hat{Q}$ Corresponding to Observed and Estimated Discharge, Respectively

Metric	
RRMSE	$\sqrt{\frac{1}{N}\sum_{i=1}^{N}\left(\frac{Q_i-\hat{Q}_i}{Q_i}\right)^2}$
NRMSE	$\sqrt{\frac{1}{N}\sum_{i=1}^{N}\left(\frac{Q_i-\hat{Q}_i}{\bar{Q}}\right)^2}$
rBias	$\frac{1}{N}\sum_{i=1}^{N}\left(\frac{Q_i-\hat{Q}_i}{Q_i}\right)$
KGE	$1-\sqrt{(\rho-1)^2+\left(\frac{\mu_Q}{\hat{\mu_Q}}-1\right)^2+\left(\frac{\sigma_Q}{\hat{\sigma_Q}}-1\right)^2}$
NSE	$1-\sum_{i=1}^{N}\left(Q_i-\hat{Q}_i\right)^2/\sum_{i=1}^{N}\left(Q_i-\bar{Q}\right)^2$

4. Experimental Design

We performed four sets of experiments, each one intended to evaluate the impact of hydraulic geometry constraints and formulations on the assimilation of SWOT satellite observations. In each experiment, different configurations of the SAD algorithm were implemented and evaluated in terms of the accuracy of river discharge estimation. These experiments included (1) the simplified assumption of rectangular river channel cross sections; (2) using channel cross sections with an empirical but generic r parameter; (3) deriving the r parameter utilizing our geomorphological classification scheme; (4) the inclusion of equations (5)–(7) as observational constraints in the assimilation. The different configurations of the SAD algorithm are also shown graphically in Figure 4 as a flow diagram.

We used the dataset from Durand et al. (2016), which includes the output from hydrodynamic model simulations of 18 rivers, to evaluate different configurations of the SAD algorithm. The physical characteristics of the rivers covered a wide range in terms of length (11 to 223 km), flow (150 to 12,160 m^3/s), drainage area (7,495 to 2,369,369 km^2), and maximum width (98 to 15,673 m). Synthetic SWOT observations were generated from the output of the hydrodynamic simulations that included daily values of spatially variable water surface elevation (i.e., longitudinal profiles), slope, and top width corresponding to different flows. These data were simulated after forcing the different models with in situ channel bathymetry, model-derived or observed inflows, and water elevation as upstream and downstream boundary conditions, respectively. Validation results of these models showed that they realistically reproduced water surface elevation and inundation extent (e.g., Jung et al., 2012), making them appropriate for the purpose of evaluating river discharge from SWOT-like satellite observations. The synthetic SWOT observations were derived by adding zero-mean Gaussian errors (temporally uncorrelated) to the observables with standard deviations of 5 cm, 5 m, and 0.1 cm/km for water surface elevation, width, and slope, respectively. Prior probability distributions were estimated for discharge, bed elevation, channel roughness, and the channel geometry parameter (r) using the SWOT synthetic observations and methods described in sections 2.3 and 3. Other inputs to the GVF model included the bankfull width and depth, which were calculated as the maximum observed surface water width and elevation, respectively, after subtracting the assumed bed elevation (derived from the prior PDF that is estimated) for the latter.

The performance of the different configurations of the SAD algorithm was evaluated with five metrics (Table 3) including relative root mean squared error (RRMSE), normalized root mean squared error (NRMSE), relative bias (rBias), Kling-Gupta efficiency (KGE), and Nash-Sutcliffe efficiency (NSE). RRMSE, NRMSE, and rBias can help characterize the deviation and mean of the model residuals and despite their shortcomings (e.g., Ehret & Zehe, 2011) are some of the most widely used error metrics (Dawson et al., 2007). NSE is another widely used goodness-of-fit metric that quantifies the portion of the observed variance explained by the model. Finally, the KGE presents a decomposition of the NSE that facilitates analysis of different components of the hydrologic signal into the Pearson correlation (ρ) between observations and model predictions and the ratios of the means and standard deviations of observations (μ_Q and σ_Q) and model predictions ($\hat{\mu_Q}$ and $\hat{\sigma_Q}$) (Gupta et al., 2009).

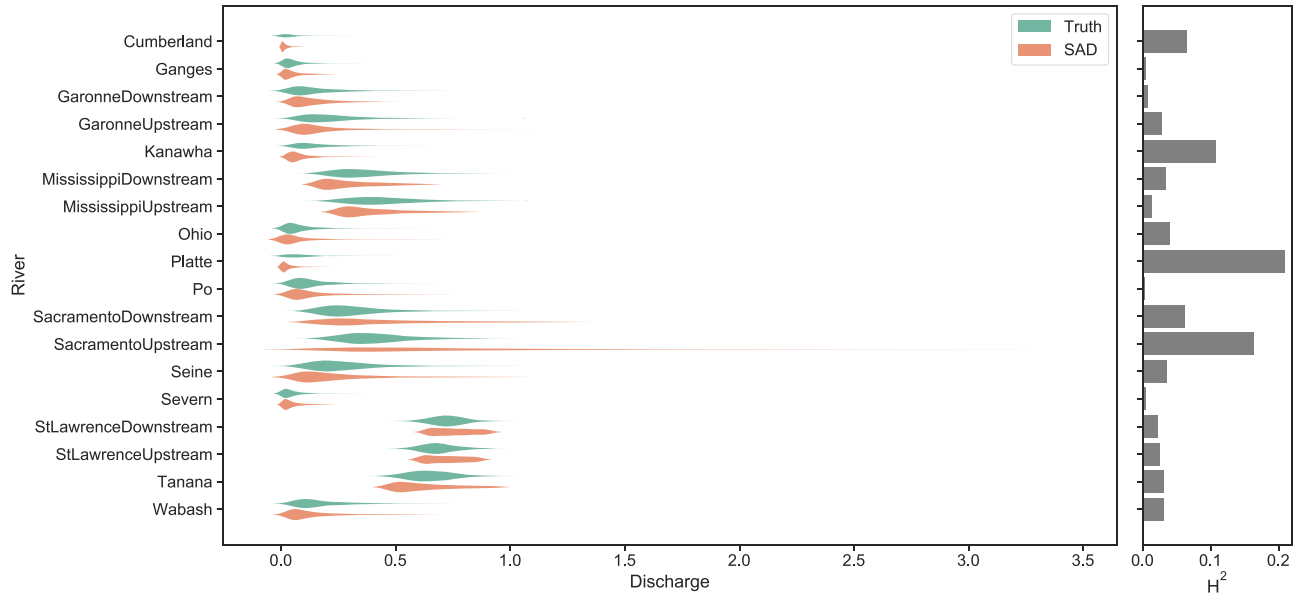

Figure 5. Empirical and estimated prior distributions of river discharge (normalized by each river's "truth" maximum values for display purposes) for each river case study. Also shown is the Hellinger distance metric between the two distributions of each river (smaller values indicate higher degree of similarity).

Given the importance of prior information to the performance of any Bayesian scheme (Hagemann et al., 2017), we examined whether the method of deriving prior PDFs that is part of the SAD algorithm can reproduce the observed distribution of river discharge. Note that this method of deriving a prior PDF is part of all four configurations of the SAD algorithm implemented and evaluated in our study. Apart from visually comparing the two distributions, we can quantitatively assess their similarity using an f-divergence metric. Here we choose the Hellinger distance that is bounded between 0 and 1 and can be considered the probabilistic equivalent of the commonly used Euclidean distance (Cam & Yang, 2000). The Hellinger distance between two probability distributions with densities $f(x)$ and $g(x)$ can be expressed as $H^2 = 1 - \int \sqrt{f(x)g(x)}dx$ (Pollard, 2002). If we assume that the two probability distributions are lognormal, a good approximation in the case of river discharge, H, can be practically calculated from

$$H^2 = 1 - \sqrt{\frac{2\sigma_1\sigma_2}{\sigma_1^2 + \sigma_2^2}} exp\left[-\frac{(\mu_1 - \mu_2)^2}{4(\sigma_1^2 + \sigma_2^2)}\right] \tag{9}$$

where μ and σ are the means and standard deviations of the two log-transformed distributions.

5. Results

5.1. Prior Distributions

Figure 5 shows the comparison of the empirical PDF derived from the "true" discharge and the estimated prior PDF used in the SAD assimilation algorithm. The comparison is shown in the form of a set of violin plots that correspond to the probability densities grouped for each river. The discharge values have been normalized by each river's "true" maximum value in order to display the PDFs of all the case studies on a single plot. With the exception of the Upstream Sacramento River, SAD appears to reproduce the range of the prior distribution of discharge. The mode and shape, including dispersion and skewness, were captured well in the cases of the Ganges, Upstream Garonne, Ohio, Po, Severn, and Wabash Rivers. On the other hand, the priors for the rest of the case studies were not able to reproduce some of the properties of the observed distribution as well, potentially affecting the efficacy of the data assimilation algorithm. The similarity between the estimated prior distribution and the corresponding truth that was illustrated in Figure 5 was also confirmed by the Hellinger distance metric for each river. The computed Hellinger distances ranged from 0.002 (Po River) to 0.209 (Platte River) and a median value of 0.031, suggesting that the SWOT observations and rejection sampling method led to an informative prior.

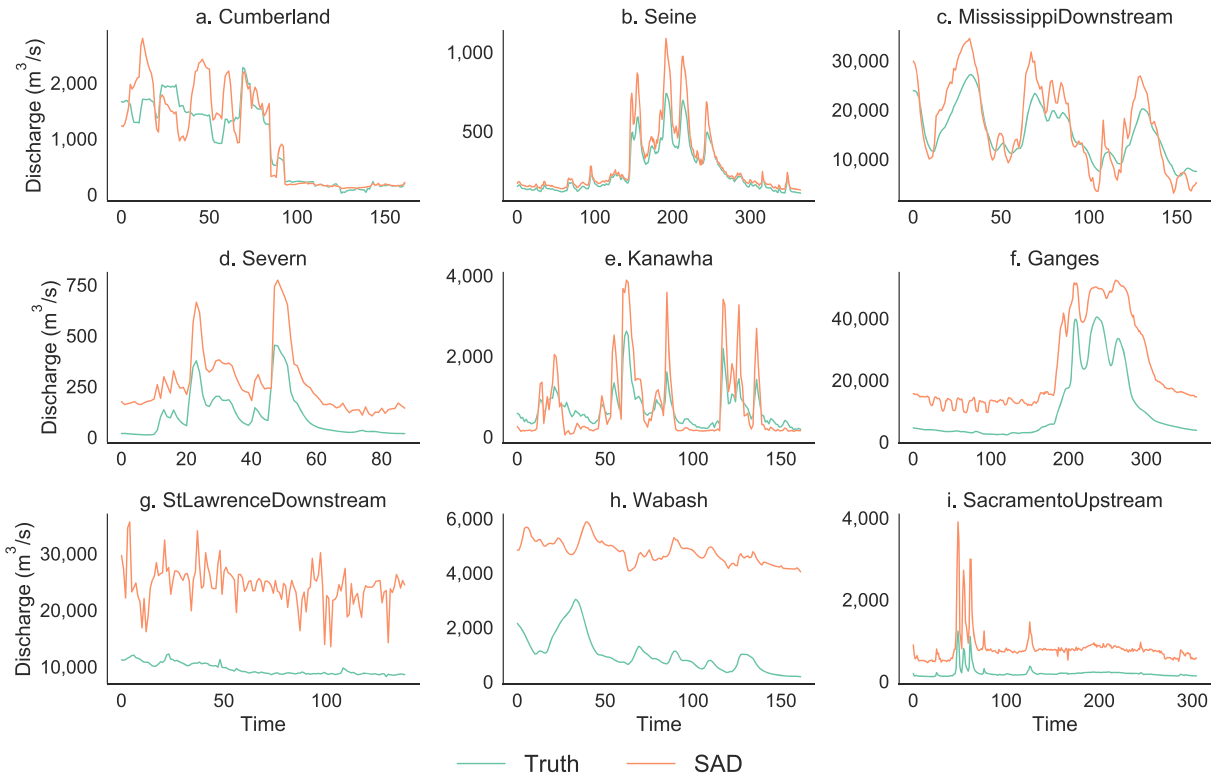

Figure 6. Hydrographs from the SAD algorithm when assuming a rectangular cross section compared to true discharge for selected rivers.

5.2. Rectangular Channel

Discharge estimation approaches from remote sensing observations that employ hydraulic models globally utilize the assumption of a rectangular channel in the absence of other data (e.g., Yoon et al., 2012). Therefore, the first experiment we performed involved making this approximation for the channel cross sections by setting r to a very high value (1e6), in the GVF model. From the geomorphological classification, most of the rivers do not appear to be well represented as a rectangular channel. Nonetheless, the SWOT observations could contain adequate information to compensate for uncertainty in the forward model. Figure 6 shows hydrographs (from a subset of the river case studies) of the SAD-estimated discharge when using the rectangular channel approximation compared to the true discharge (the comparison hydrographs from all rivers can be found in the supporting information, Figure S2). In some cases, the assimilation is able to reproduce discharge with reasonable accuracy despite the simplified channel geometry. In particular, the Cumberland and the Seine showed relatively high efficiencies with NSE of 0.69 and bias of −16%. The St Lawrence Upstream and both Mississippi River reaches also showed relatively good performance with RMSEs between 24.3% and 41.3%. For the rest of the cases, the performance of SAD with a rectangular channel ranged from capturing the temporal variability with some bias (e.g., the Po, Severn, and Sacramento) to completely missing the discharge dynamics (e.g., the downstream Garonne, and St Lawrence Rivers). The largest relative biases in the rectangular channel estimates are found for the Tanana, Wabash, Severn, upstream Sacramento, and Ganges with values ranging from −224% to −604%. Overall, only 6/18 rivers had a positive NSE, ranging from 0.12 to 0.69, 12/18 had a positive KGE, ranging from 0.06 to 0.76, and 5/18 had NRMSE or RRMSE below 50%, ranging from 19% to 48%. The rivers with the worst negative NSEs were the Wabash (−31.7), the upstream Sacramento (−26.1), the Tanana (−24.4), and the downstream St Lawrence (−213.8). Interestingly, the Tanana had a positive KGE value, which was reflected by RMSEs that were better than the other "worst-NSEs" rivers (73% versus 157% to 376% in terms of NRMSE). The median values for the error metrics were 0.11 for the KGE, −0.46 for the NSE, 75% for the NRMSE, 97% for the RRMSE, and −83% for the relative bias. These relatively poor results suggest the inappropriateness of the rectangular channel approximation, although the algorithm might be compensating for this poor approximation in some cases by estimating an effective bed elevation and channel roughness.

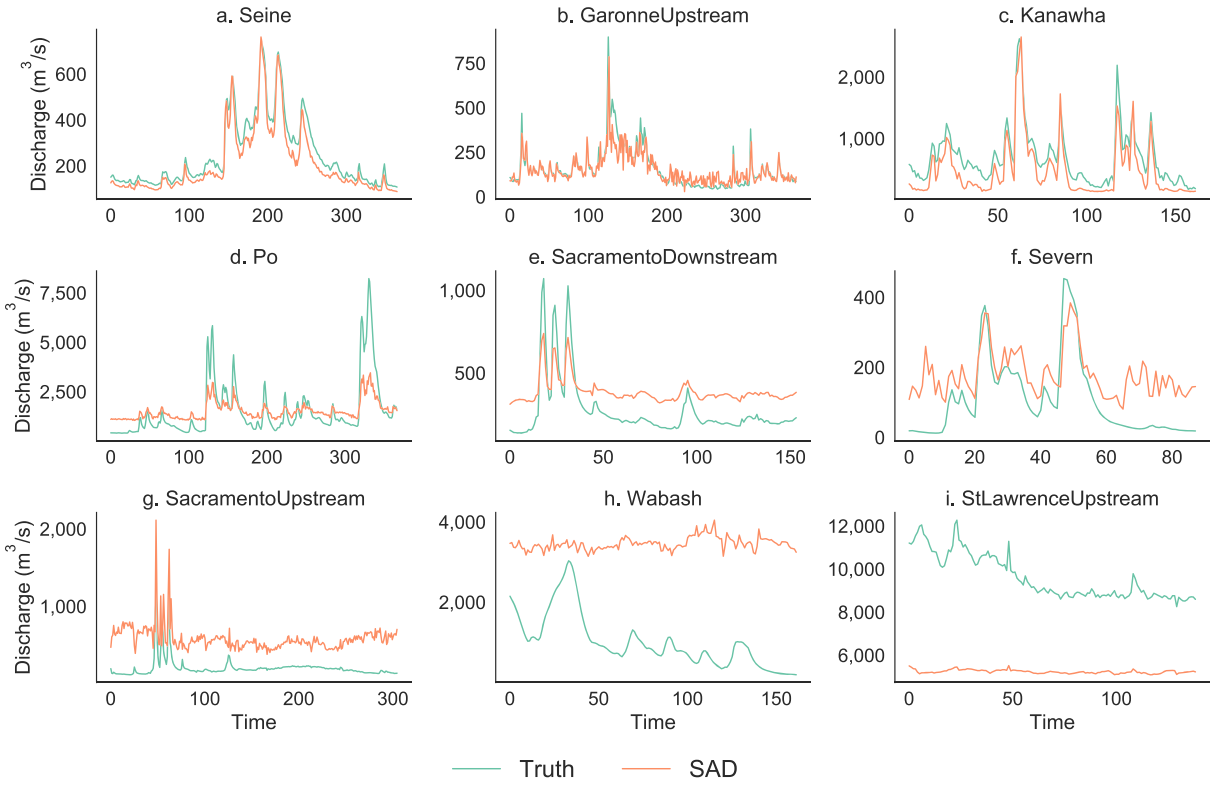

Figure 7. As Figure 6, but for the SAD algorithm configuration using hydraulic geometry relations with a generic *r* parameter.

5.3. AHG Channel

In order to improve on the river channel representation in the GVF forward model, we used the HYDRoSWOT dataset to estimate a more realistic *r* shape parameter. The second experiment we performed derived a distribution of *r* from the entire HYDRoSWOT dataset, ignoring any information on the classification of each river. From the histogram of the data, a log-normal distribution appeared to be a good fit, and the resulting parameters were $\mu = 0.95$ and $\sigma = 1.02$ for the prior probability distribution of *r*. Figure 7 shows time series of the true and SAD-estimated discharge when using a river channel with an *r* parameter sampled from this generic log-normal distribution for selected rivers, along with the a scatter plot comparing daily discharge values for all rivers (hydrographs from all rivers are shown in the supporting information, Figure S4).

The generic *r* parameter improved the discharge estimation accuracy for 13/18 rivers, with the exceptions being the Cumberland, Platte, downstream Sacramento, Tanana, and upstream St Lawrence. For the cases where improvement occurred, the median KGE increased from 0.06 to 0.33, the NSE from −0.42 to 0.51, while the NRMSE and RRMSE decreased from 85 and 107% to 43 and 71%, respectively. In contrast, the performance metrics worsened for the five other rivers, with median values of KGE decreasing from 0.31 to −0.06, NSE from −1.02 to −1.54, and RRMSE increasing from 73 to 80%. Somewhat surprisingly, the NRMSE actually decreased for the five rivers with worse performance (66% to 57%). In the case of the Cumberland, the generic *r* configuration of SAD does not perform well during the first half of the simulation period when river slope was steeper than about 0.1 cm/km (Durand et al., 2016). Moreover, this configuration of the algorithm did not estimate the flow peaks for the downstream Sacramento and also lost some or all of the dynamic information for the Platte and upstream St Lawrence. On the other hand, the volume errors appeared to be reduced when a generic *r* parameter was introduced. For example, the Severn NRMSE was reduced from 158% to 92% while the corresponding numbers for the downstream St Lawrence were 157% and 36%, respectively. Overall, this alternative approximation for channel geometry led to an improvement, with the median relative bias decreasing to −39%, NRMSE/RRMSE decreasing to 49/77%, and NSE and KGE increasing to 0.31 and 0.33, respectively.

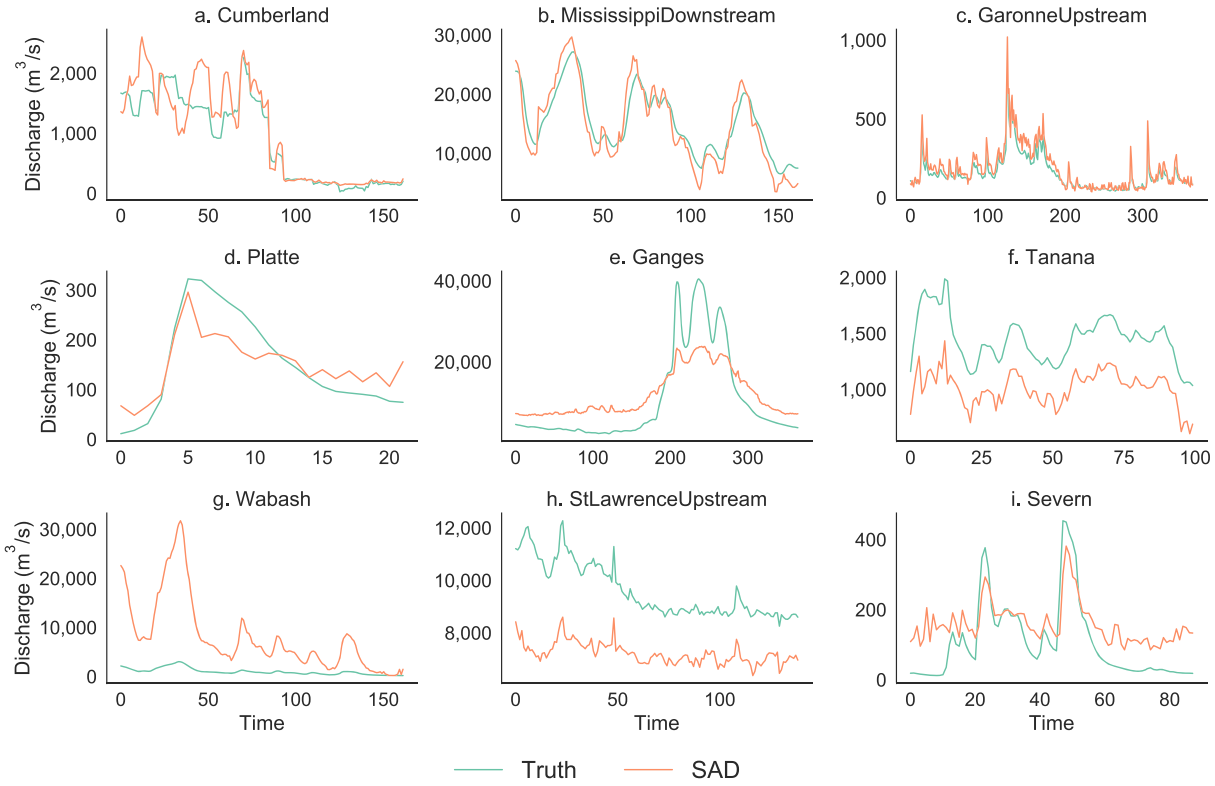

Figure 8. As Figure 6, but for the SAD algorithm configuration using hydraulic geometry relations with a *r* parameter derived from a geomorphological classification.

Despite the improvement in discharge estimation accuracy, the generic *r* is another approximation similar to the rectangular channel assumption and does not exploit any of the information from the river's geomorphology or observations to derive an improved prior probability distribution for *r*. Utilizing the geomorphological classification framework, we can introduce prior knowledge to aid in the inference of the unobservable channel geometry. Ideally this geomorphological information would allow the SAD algorithm to derive a PDF (via the rejection sampling approach) for the *r* parameter that has the correct support and is less dispersed. Figure 8 shows the comparison (similar format as Figures 6 and 7, with all hydrographs shown in the supporting information Figure S5) between true and SAD-estimated discharge time series, with the latter using a *r* parameter distribution estimated from the geomorphological classification framework.

This geomorphological *r* (Gr hereafter) configuration improves the accuracy of the estimated discharge for 13/18 rivers (not the same as before) while slightly decreasing accuracy for three rivers. The Seine and the Wabash are the two rivers where performance is worse across all error metrics. The Gr estimation overpredicts the peak flows for the Seine river and overestimates the flow volume for the Wabash despite better capturing the temporal dynamics (compared to the generic *r*). The largest improvements in terms of efficiency were the upstream Sacramento, the Platte, and the Tanana, with increases in the NSE of 12.9, 2.3, and 26.5, respectively (corresponding values for KGE were 1.6, 0.6, and 0.7). The Gr configuration was able to much better reproduce the temporal dynamics in both St Lawrence reaches, despite not being able to entirely remove the bias in these cases. In other rivers where improvement occurred, the Gr hydrograph did not exhibit the same high-frequency variability that the generic *r* configuration showed, with both the upstream and downstream Mississippi reaches being the most prominent cases of that behavior. The Ganges is an interesting case because the rectangular assumption led to consistent overestimation of discharge whereas both the generic *r* and Gr configurations overestimated the low flows but underestimated the periods of peak flow, consistent with results from other algorithms (Durand et al., 2016). Overall, the Gr configuration improved the error metrics compared to both the generic *r* and rectangular channel approximations, with the median KGE and NSE being 0.57 and 0.66, while the RMSEs and bias were reduced to 35%/52% (NRMSE/RRMSE) and −19%, respectively.

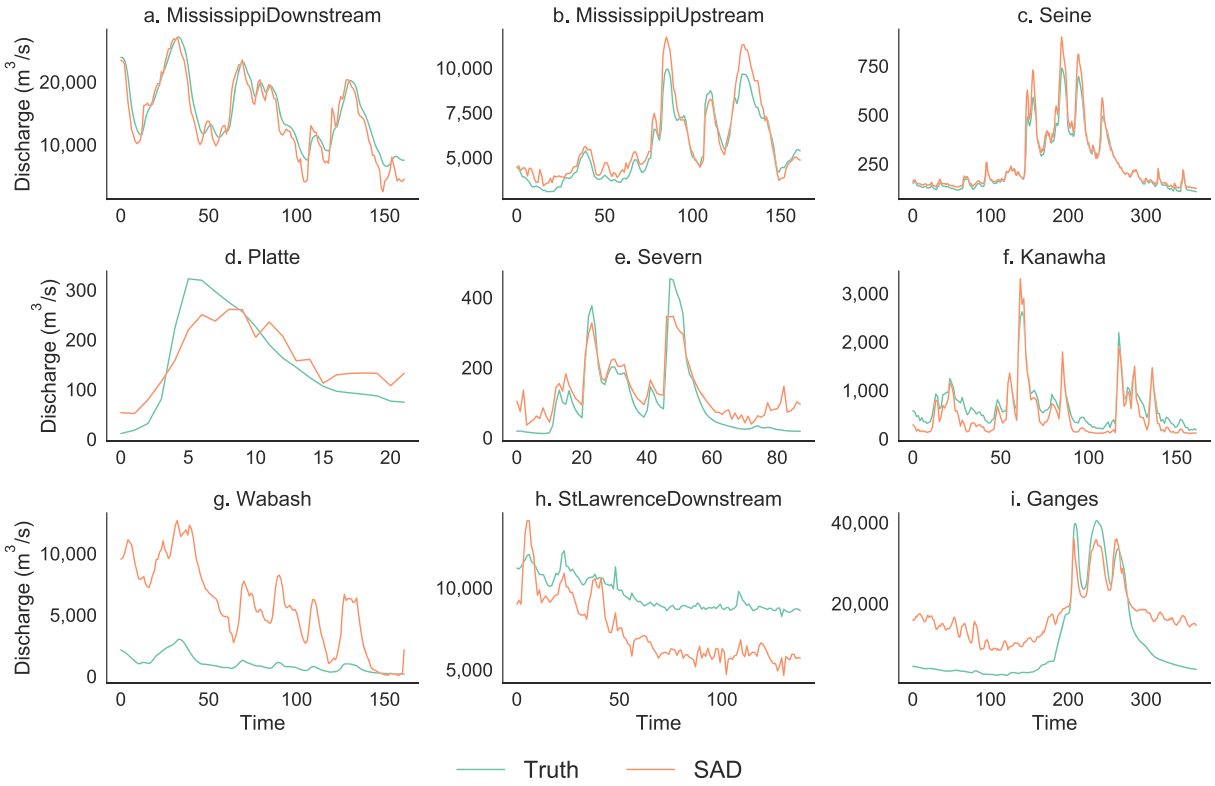

Figure 9. As Figure 6, but for the SAD algorithm configuration using hydraulic geometry relations with a *r* parameter derived from a geomorphological classification and applying the AHG regularization.

5.4. AHG Constraints

We performed a fourth experiment to evaluate the impact of applying a regularization step before the assimilation of SWOT observations. The regularization explicitly incorporated the AHG power laws into the discharge estimation, which essentially "tightens" and potentially shifts the prior distribution of discharge that was used to generate the ensemble for the standard assimilation of the SWOT observations. We used an identical configuration in the forward modeling with the geomorphological *r* experiment; therefore, the only difference was the preconditioning of the prior discharge ensemble through regularization with the AHG relationships. Figure 9 shows hydrographs for a representative (in terms of performance) subset of rivers of the true and SAD-estimated discharge, with the latter estimate incorporating the AHG regularization, along with a scatter plot of true and SAD-estimated daily discharge for all rivers (hydrographs of all rivers are shown in the supporting information, Figure S6).

The AHG-constrained configuration (hereafter AHGc) improved the accuracy of the discharge estimates for 13/18 rivers but degraded performance for five rivers. The worse-performing rivers included the Tanana, Ganges, downstream St Lawrence, Po, and the downstream Sacramento, with the latter two showing a very small decrease in efficiencies (KGE from 0.58 to 0.57 for the Po and 0.43 to 0.40 for the downstream Sacramento). The Tanana shows a relatively small degradation in terms of KGE but a larger one for the rest of the error metrics (e.g., NRMSE from 31% to 47% and NSE from −3.54 to −9.38). The accuracy for the downstream St Lawrence degraded similarly across all metrics except for NSE, which increased from −7.47 to −4.87 while showing a modest increase in RMSEs. The Ganges showed a decrease in accuracy when applying the AHG constraints, but a comparison of any of the SAD configurations (RRMSE of 115% at best) with the performance of other SWOT-estimation discharge algorithms (RRMSE of 52%; Bonnema et al., 2016) suggests that either the AHG relations are limited in braided rivers or that improvements in the SAD algorithm are needed.

The improvements in discharge estimation in terms of RMSEs (for the rivers that did improve) were relatively modest with a median decrease of 8.6% and 7.8% for NRMSE and RRMSE, respectively. The largest improvement in terms of RMSEs was found for the upstream St Lawrence, with NRMSE and RRMSE being

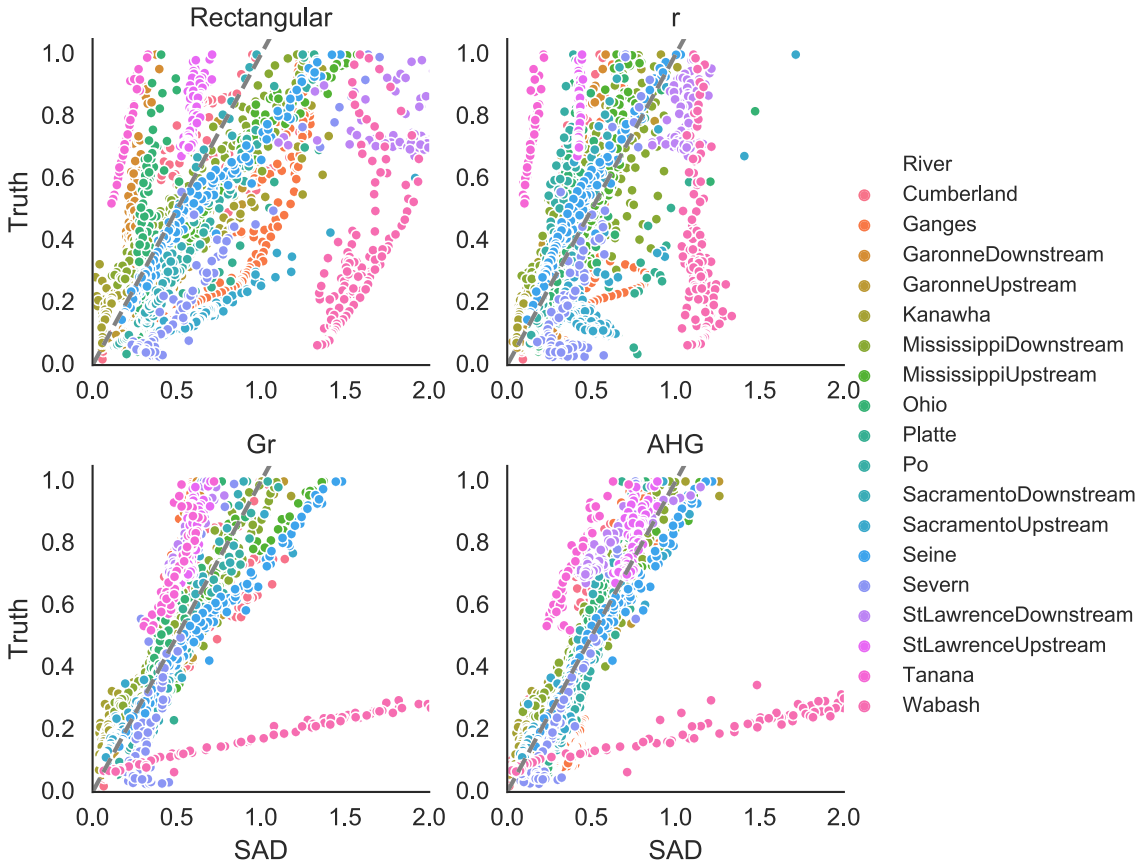

Figure 10. Scatter plots comparing true and SAD-estimated daily discharge values, for all rivers and the four channel geometries: rectangular, generic *r*, and geomorphological *r* with and without AHG constraints. Discharge values have been normalized by the maximum observed discharge for each river, in order to facilitate different flow magnitudes in the same plot. Moreover, the *x*-axis has been cut off for visual purposes.

reduced to 9.2% and 8.1%, respectively. The Seine and the Severn also showed a large improvement with the AHG constraints attenuating the overestimated peak flows and better capturing the low flow periods for both rivers. The NSEs for these two rivers increased from 0.66 to 0.93 and 0.43 to 0.80, respectively. In the cases of the two Garonne River reaches, AHGc better captured the peak flows and also reduced the errors for the descending limbs of the hydrographs (particularly evident for the upstream Garonne during days 176–279). Overall, for the rivers that did improve with the AHGc, the median increase in NSE and KGE was 0.14 and 0.12 while the NRMSE, RRMSE, and rBias exhibited a median decrease of 8.3%, 6.7%, and 7.9%, respectively.

6. Discussion

Examining the overall performance of the different configurations indicates that incorporating hydraulic geometry relations, via the river channel formulation and the AHG equations, resulted in improved discharge estimates (see Tables S2 to S7 in the supporting information). The improvement is evident when examining Figure 10, which shows scatter plots of true and SAD-estimated daily discharge from all rivers for the different algorithm configurations: the rectangular channel approximation (Rect), the generic *r* parameter (r), incorporating the geomorphological classification (Gr), and including the regularization with the AHG constraints (AHG). The scatter was reduced as hydraulic geometry relations are added to the forward model and the assimilation, with the exception of the Wabash River, where adding the AHG constraints degraded discharge estimation accuracy. A different way of comparing the different SAD configurations is shown in Figure 11, which displays boxplots of the discharge error metrics for all rivers. The median NSE increased with the addition of constraints and information to the estimation: −0.46 for Rect, 0.31 for r, 0.66 for Gr, and 0.77 for AHG. The performance in terms of NSE appeared more consistent for Rect than the generic *r*, with a smaller range of efficiencies despite the median value being lower. This could be attributed

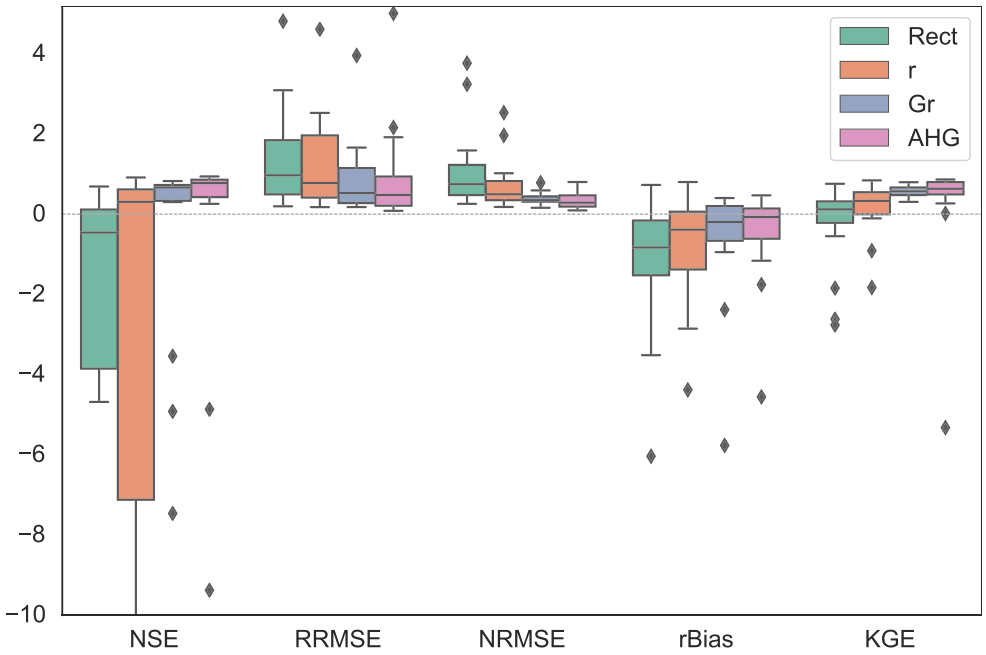

Figure 11. Boxplot of discharge error metrics from all case studies for the different algorithm configurations, including rectangular channel (Rect), generic *r* parameter (r), *r* parameter derived from the geomorphological classification (Gr), and same as Gr but with the AHG regularization applied. Range of *y*-axis values has been cut off for display purposes.

to the variance of the prior *r* distributions for each approximation. The range of *r* values for the Rect distribution was large and led to a practically identical channel shape, while the range of *r* values in the generic distribution led to significantly varying channel shapes affecting the forward model predictions. The AHG configuration had only three rivers with negative NSEs, compared to 12 for Rect, 6 for r, and 4 for Gr.

The same pattern was observed in terms of performance for both RMSE metrics, with AHG having the smallest median errors of 28.6% (NRMSE) and 47.9% (RRMSE). Moreover, the RMSEs decreased as the incorporation of hydraulic geometry relations is enhanced. The median values for the NRMSE (RRMSE) were 74.5% (96.8%) for Rect, 49.4% (77.3%) for r, and 34.7% (52.4%) for Gr. Both the Gr and AHG configurations had a smaller variance of RMSEs compared with the more generic river channel approximations, as evidenced by the interquartile ranges. The distributions of RMSEs were relatively skewed for all configurations, with some rivers underperforming for the AHG. Given that the flow depth (difference between the water surface and bed elevations) was assimilated essentially twice (once with equation (6) and then again with the SWOT observation), any errors in the SAD-estimated bed elevation lead to volume errors being worse for some rivers when the additional AHG constraints are applied.

The AHG also outperformed the other three configurations in terms of both relative bias and KGE. The median bias showed that all configurations were negatively biased, although the AHG had the smallest value (−7.4%) while Rect had −83.3%, r had −38.9%, and Gr had a rBias of −19.5%. There were only two rivers where SAD-estimated discharge was consistently positively biased, the Kanawha and the upstream St Lawrence, although the latter had a relatively small bias of 4.9% for the AHG. The KGE metric generally showed that all four configurations had reasonable performance, with consistent ranges of KGE values between the generic river channel approximations. As the application of hydraulic geometry was enhanced, KGE increased with the median values being 0.12 for Rect, 0.33 for r, 0.57 for Gr, and 0.63 for AHG.

Apart from the traditional error metrics, we also examined the performance of the different configurations of the SAD algorithm and the impact of the hydraulic geometry constraints using several other indicators. The latter included the time to peak discharge (averaged if multiple events were present in the time series) and the hydrograph volume (Figure S6 in the supporting information shows comparisons of mean time to peak discharge and flow volume between observations and the four SAD estimates). The AHG configuration showed the best overall performance in terms of predicting time to peak discharge, with a NSE value of 0.67 compared to 0.58, 0.61, and 0.42 of the Gr, r, and rectangular channel configurations, respectively. In terms of

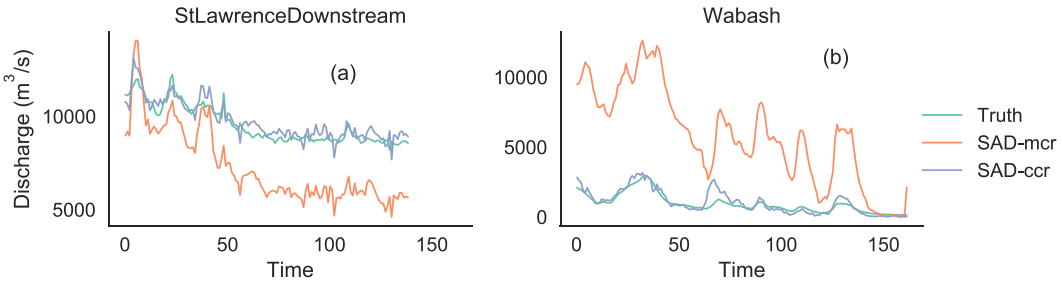

Figure 12. Hydrographs of true and SAD-estimated discharge with AHG regularization and misclasssified (SAD-mcr) and correctly classified (SAD-ccr) r parameter for the downstream St Lawrence (a) and Wabash (b) Rivers.

flow volume, all SAD configurations perform almost equally well with the r, Gr, and AHG estimates having NSE values of 0.73, 0.90, and 0.65 compared to −0.55 for the rectangular channel formulation.

Although overall the geomorphological classification improved the discharge estimated from the assimilation, a misclassification could limit the effectiveness of the assimilation and/or the AHG constraints. The initial impact of a misclassification would manifest in the erroneous truncation of the prior distribution for the r parameter and would propagate to the the GVF model, leading to a potentially poor estimate of the model-observation difference and model covariance. We tested this hypothesis by noting that there were two rivers (Wabash and downstream St Lawrence) where the SAD algorithm consistently underperformed despite increasing application of the AHG constraints. After changing their classification and applying SAD with the AHG configuration, we found that the best results were obtained for $r \in (0, 1]$. Figure 12 shows hydrographs of the true and SAD-estimated discharge for the downstream St Lawrence and Wabash when using the geomorphologically classified (SAD-mcr) and new r (SAD-ccr). The smaller r bounds led to significantly improved discharge for both rivers, with efficiencies being 0.68 (NSE) and 0.69 (KGE) for the Wabash and 0.79 (NSE) and 0.91 (KGE) for the St Lawrence. The "misclassified" NSEs (KGEs) were −69.7 (−5.33) for the Wabash and −4.87 (0.01) for the downstream St Lawrence.

Despite the simplicity of the GVF model, which makes properly handling complex rivers difficult, these streams could be approximated by estimating effective channel geometries (via the r parameter) that reproduce the observed width and WSE profiles. However, if the channel shape parameter r is not commensurate with that approximation, the assimilation algorithm would be hindered due to the erroneous predictions from the forward model. On the other hand, a reason that the $r < 1$ produced better results for the downstream St Lawrence and the Wabash could be the maximum "observed" width. The Wabash and downstream St Lawrence have the largest maximum widths from the rivers that were not classified as braided (11,791 m and 15,673 m, respectively, in the simulated dataset). Since the maximum observed width is used as the bankfull width in the GVF model, the smaller r could be compensating for the evident overestimation in channel width (even if the classification was correct).

Finally, we examined whether the regularization with the AHG constraints led to estimates of discharge that corresponded to empirical AHG coefficients convergent with their theoretical values (given by equations (5)–(7). We estimated the coefficients via linear regression of the logarithms of the AGH discharge and the GVF-predicted flow depth, width, and velocity. Because we used a spatially uniform r channel shape parameter (i.e., the exponents in the AHG equations are identical along each river), we only calculated and compared the coefficients at the downstream cross sections (shown graphically in Figure S7 in the supporting information). The width AHG relationship appears to agree best in terms of the theoretical values of the exponent b and coefficient a with an R^2 of 0.98 and 0.99, respectively. This agreement is reasonable given that width is directly observed and indirectly used in the assimilation via the forward model predictions. In contrast, the agreement is rather poor for the flow depth exponent f and coefficient c, with a R^2 of 0.14 and 0.18, respectively. The bed elevation values that are estimated from SAD are used in both the regularization and assimilation steps, and any errors in that estimation could lead to divergent results in the $Q - y$ regression from the theoretical values. Furthermore, the regularization that was applied essentially amounts to modifying the discharge prior ensemble to weakly impose the AHG constraints (Sugiura et al., 2013), and therefore, the assimilation could have resulted in a discharge solution that is not consistent with the preceding applied AHG constraint. The velocity exponent m and coefficient k appear to have a modest

agreement with their theoretical values, with a R^2 of 0.51 and 0.56, respectively, which is reasonable given that velocity depends on both flow depth and width.

7. Conclusions

The upcoming SWOT satellite mission will offer a unique opportunity to map river discharge at an unprecedented spatial resolution globally from its observations of water surface elevation, width, and slope. Since river discharge will be indirectly observed from SWOT, a number of algorithms have been developed with varying complexity to estimate discharge from SWOT observables. During the implementation and evaluation of these algorithms, some issues arose that motivated the approach presented in this study (SAD). Data assimilation has a long history of successful application to SWOT (or SWOT-like) observations and therefore was used as the base to build a new algorithm. SAD was developed by combining a physically based and data-driven approach to estimate the prior probability distributions needed for the assimilation of the SWOT observations. The data-driven components of SAD were based on a rejection sampling approach as well as a geomorphological classification framework, while hydraulic geometry relationships were incorporated into the algorithm to ameliorate issues of parameter equifinality by further constraining the estimation problem. The comprehensive dataset first used in Durand et al. (2016) allowed for evaluating the integration of hydraulic geometry relations with data assimilation of SWOT observations. A set of four experiments that progressively added the AHG constraints onto a simple rectangular channel assumption were performed, with the configuration that incorporated the full set of AHG constraints giving the most consistent results in terms of discharge estimation, as evidenced when examining five error metrics.

We contend that the results above represent excellent performance for a discharge algorithm that does not invoke any in situ data. In order to contextualize the development and implementation of the SAD algorithm, we can draw upon the discussion found in Durand et al. (2016), which compared the performance of five discharge algorithms. Our goal here is not to explicitly assess whether SAD outperformed other SWOT discharge estimation algorithms or suggest that SAD alone should be used moving forward. The lessons learned from that paper have directly influenced the development of SAD. The configuration of the SAD algorithm that included the entirety of the hydraulic geometry constraints led to a positive NSE for all rivers except for the Tanana River, so we examined potential reasons for the consistent performance across varying river environments and flow regimes. We observed from the other algorithm results that synergy among them could prove fruitful. That is, merging the best elements of each algorithm could combine elegantly to yield more consistent performance. Thus, we were inspired by the hydraulic geometry of AMHG (later to become BAM, Bayesian AMHG Manning) and MFG (Mean Flow and Geomorphology), the Manning's inversion of GaMO and MetroMan, the data assimilation in GaMO, and the Markov chain of MetroMan and BAM. The different components of the SAD algorithm as implemented here have a direct correspondence with these elements from each of the other SWOT discharge algorithms. Durand et al. (2016) suggested that the addition of a priori information should improve the effectiveness of each algorithm, while a hybrid or synergistic approach could lead to a SWOT discharge product viable for rivers globally. Our data-driven derivation of prior probability distributions was able to generate informative priors from just the SWOT observations and a mean annual flow, following directly from this suggestion and leading to an algorithm that performs consistently well across different riverine environments.

Despite the encouraging results from the evaluation of SAD with a comprehensive albeit synthetic dataset, a number of limitations need to be addressed through future work. Recent work has utilized airborne measurements from AirSWOT, a SWOT-like airborne Ka-band radar, to estimate hydraulic variables (Altenau et al., 2017; Tuozzolo et al., 2019). These datasets could potentially be used to test and evaluate SAD to complement the analysis presented here. Furthermore, the at-many-stations hydraulic geometry (AMHG) which is an extension to the classic AHG theory showed that the empirical parameters of AHG (valid at cross-sections) are functionally related along a river (Gleason & Wang, 2015). The incorporation of AMHG could lead to further constraining the prior and posterior distributions of river discharge, as it is reconcilable with AHG (Brinkerhoff et al., 2019), making AMHG a promising approach for an algorithm such as SAD. Alternatively, other discharge estimation approaches that only depend on hydraulic geometry relations (e.g., Dingman & Sharma, 1997; López et al., 2007) Finally, the implementation of the SAD algorithm presented here is not applicable to an entire river network because it does not take into account any flows at junctions or from lateral tributaries. Given that the objective of this study was the evaluation of hydraulic

geometry constraints on the assimilation of SWOT satellite observations, the aspects of an operational implementation of the algorithm were considered to be beyond the scope of this study. Nonetheless, there are a number of approaches that could be used to enable the application of SAD over river networks (e.g., Zhu et al., 2011).

Acknowledgments
Funding for this work was provided by the NASA SWOT Science Team and Terrestrial Hydrology programs. The authors would like to thank Renato Frasson and Michael Durand for providing the dataset used in this study. Data and software code used to generate the results presented herein can be found at https://figshare.com/articles/SWOT_Assimilated_DiScharge/10032311.

References

Altenau, E. H., Pavelsky, T. M., Moller, D., Lion, C., Pitcher, L. H., Allen, G. H., et al. (2017). AirSWOT measurements of river water surface elevation and slope: Tanana River, AK. *Geophysical Research Letters*, *44*, 181–189. https://doi.org/10.1002/2016GL071577

Andreadis, K. M., Clark, E. A., Lettenmaier, D. P., & Alsdorf, D. E. (2007). Prospects for river discharge and depth estimation through assimilation of swath-altimetry into a raster-based hydrodynamics model. *Geophysical Research Letters*, *34*, L10403. https://doi.org/10.1029/2007GL029721

Ashmore, P., & Sauks, E. (2006). Prediction of discharge from water surface width in a braided river with implications for at-a-station hydraulic geometry. *Water Resources Research*, *42*, W03406. https://doi.org/10.1029/2005WR003993

Biancamaria, S., Durand, M., Andreadis, K. M., Bates, P. D., Boone, A., Mognard, N. M., et al. (2011). Assimilation of virtual wide swath altimetry to improve Arctic river modeling. *Remote Sensing Environment*, *115*(2), 373–381. https://doi.org/10.1016/j.rse.2010.09.008

Biancamaria, S., Lettenmaier, D. P., & Pavelsky, T. M. (2016). The SWOT mission and its capabilities for land hydrology. *Surveys in Geophysics*, *37*(2), 307–337. https://doi.org/10.1007/s10712-015-9346-y

Bjerklie, D. M., Birkett, C. M., Jones, J. W., Carabajal, C., Rover, J. A., Fulton, J. W., & Garambois, P.-A. (2018). Satellite remote sensing estimation of river discharge: Application to the Yukon River Alaska. *Journal of Hydrology*, *561*, 1000–1018. https://doi.org/10.1016/j.jhydrol.2018.04.005

Bjerklie, D. M., Dingman, S. L., & Bolster, C. H. (2005). Comparison of constitutive flow resistance equations based on the Manning and Chezy equations applied to natural rivers. *Water Resources Research*, *41*, W11502. https://doi.org/10.1029/2004wr003776

Blasone, R.-S., Vrugt, J. A., Madsen, H., Rosbjerg, D., Robinson, B. A., & Zyvoloski, G. A. (2008). Generalized likelihood uncertainty estimation (GLUE) using adaptive Markov chain Monte Carlo sampling. *Advances in Water Resources*, *31*(4), 630–648. https://doi.org/10.1016/j.advwatres.2007.12.003

Bonnema, M. G., Sikder, S., Hossain, F., Durand, M., Gleason, C. J., & Bjerklie, D. M. (2016). Benchmarking wide swath altimetry-based river discharge estimation algorithms for the Ganges river system. *Water Resources Resources*, *52*, 2439–2461. https://doi.org/10.1002/2015WR017296

Brinkerhoff, C. B., Gleason, C. J., & Ostendorf, D. W. (2019). Reconciling at-a-station and at-many-stations hydraulic geometry through river-wide geomorphology. *Geophysical Research Letters*, *46*, 9637–9647. https://doi.org/10.1029/2019GL084529

Budd, C. J., Freitag, M. A., & Nichols, N. K. (2011). Regularization techniques for ill-posed inverse problems in data assimilation. *Computers and Fluids*, *46*(1), 168–173. https://doi.org/10.1016/j.compfluid.2010.10.002

Cam, L. L., & Yang, G. L. (2000). *Asymptotics in statistics: Some basic concepts, Springer Series in Statistics* (2nd ed.). New York: Springer-Verlag.

Canova, M., Fulton, J. W. G., & Bjerklie, D. M. (2016). USGS HYDRoacoustic dataset in support of the Surface Water Oceanographic Topography satellite mission (HYDRoSWOT) (*techreport*): U.S. Geological Survey. https://doi.org/10.5066/f7d798h6

Chevalier, L., Desroches, D., Laignel, B., Fjørtoft, R., Turki, I., Allain, D., et al. (2019). High-resolution SWOT simulations, of the macrotidal Seine estuary in different hydrodynamic conditions. *IEEE Geoscience and Remote Sensing Letters*, *16*(1), 5–9. https://doi.org/10.1109/LGRS.2018.2862470

Chow, V. T. (1955). Integrating the equation of gradually varied flow. *Proceedings of American Society of Civil Engineer*, *81*(11), 1–32.

Church, M. (2006). Bed material transport and the morphology of alluvial river channels. *Annual Review of Earth and Planetary Sciences*, *34*(1), 325–354. https://doi.org/10.1146/annurev.earth.33.092203.122721

Coron, L., Andréassian, V., Perrin, C., Lerat, J., Vaze, J., Bourqui, M., & Hendrickx, F. (2012). Crash testing hydrological models in contrasted climate conditions: An experiment on 216 Australian catchments. *Water Resources Research*, *48*, W05552. https://doi.org/10.1029/2011WR011721

Dawson, C. W., Abrahart, R. J., & See, L. M. (2007). HydroTest: A web-based toolbox of evaluation metrics for the standardised assessment of hydrological forecasts. *Environmental Modelling & Software*, *22*(7), 1034–1052. https://doi.org/10.1016/j.envsoft.2006.06.008

Dijk, A. I. J. M. V., Brakenridge, G. R., Kettner, A. J., Beck, H. E., Groeve, T. D., & Schellekens, J. (2016). River gauging at global scale using optical and passive microwave remote sensing. *Water Resources Research*, *52*, 6404–6418. https://doi.org/10.1002/2015WR018545

Dingman, S. L. (2007). Analytical derivation of at-a-station hydraulic–geometry relations. *Journal of Hydrology*, *334*(1), 17–27. https://doi.org/10.1016/j.jhydrol.2006.09.021

Dingman, S. L., & Afshari, S. (2018). Field verification of analytical at-a-station hydraulic-geometry relations. *Journal of Hydrology*, *564*, 859–872. https://doi.org/10.1016/j.jhydrol.2018.07.020

Dingman, S. L., & Sharma, K. P. (1997). Statistical development and validation of discharge equations for natural channels. *Journal of Hydrology*, *199*(1), 13–35. https://doi.org/10.1016/S0022-1694(96)03313-6

Durand, M., Gleason, C. J., Garambois, P. A., Bjerklie, D., Smith, L. C., Roux, H., et al. (2016). An intercomparison of remote sensing river discharge estimation algorithms from measurements of river height, width, and slope. *Water Resources Research*, *52*, 4527–4549. https://doi.org/10.1002/2015WR018434

Durand, M., Neal, J., Rodríguez, E., Andreadis, K. M., Smith, L. C., & Yoon, Y. (2014). Estimating reach-averaged discharge for the River Severn from measurements of river water surface elevation and slope. *Journal of Hydrology*, *511*, 92–104. https://doi.org/10.1016/j.jhydrol.2013.12.050

Ehret, U., & Zehe, E. (2011). Series distance—an intuitive metric to quantify hydrograph similarity in terms of occurrence, amplitude and timing of hydrological events. *Hydrology and Earth System Sciences*, *15*(3), 877–896. https://doi.org/10.5194/hess-15-877-2011

Evensen, G. (2003). The ensemble Kalman filter: Theoretical formulation and practical implementation. *Ocean Dynamics*, *53*(4), 343–367. https://doi.org/10.1007/s10236-003-0036-9

Evensen, G. (2004). Sampling strategies and square root analysis schemes for the EnKF. *Ocean Dynamics*, *54*(6), 539–560. https://doi.org/10.1007/s10236-004-0099-2

Feng, D., Gleason, C. J., Yang, X., & Pavelsky, T. M. (2019). Comparing discharge estimates made via the BAM algorithm in high-order Arctic rivers derived solely from optical CubeSat, Landsat, and Sentinel-2 data. *Water Resources Research*, *55*, 7753–7771. https://doi.org/10.1029/2019WR025599

Ferguson, R. (1986). Hydraulics and hydraulic geometry. *Progress in Physical Geography: Earth and Environment*, *10*(1), 1–31. https://doi.org/10.1177/030913338601000101

Ferguson, R. (2010). Time to abandon the Manning equation? *Earth Surface Processes and Landforms*, *35*(15), 1873–1876. https://doi.org/10.1002/esp.2091

Ferguson, R. (2013). Reach-scale flow resistance. In J. Shroder (Editor in Chief), E. Wohl (Ed.) *Treatise on Geomorphology* (Vol. 9, pp. 50–68). San Diego, CA: Academic Press.

Garambois, P.-A., Calmant, S., Roux, H., Paris, A., Monnier, J., Finaud-Guyot, P., et al. (2017). Hydraulic visibility: Using satellite altimetry to parameterize a hydraulic model of an ungauged reach of a braided river. *Hydrological Processes*, *31*(4), 756–767. https://doi.org/10.1002/hyp.11033

Garambois, P.-A., & Monnier, J. (2015). Inference of effective river properties from remotely sensed observations of water surface. *Advances in Water Resources*, *79*, 103–120. https://doi.org/10.1016/j.advwatres.2015.02.007

García-Pintado, J., Mason, D. C., Dance, S. L., Cloke, H. L., Neal, J. C., Freer, J., & Bates, P. D. (2015). Satellite-supported flood forecasting in river networks: A real case study. *Journal of Hydrology*, *523*, 706–724. https://doi.org/10.1016/j.jhydrol.2015.01.084

Gleason, C. J. (2015). Hydraulic geometry of natural rivers: A review and future directions. *Progress in Physical Geography: Earth and Environment*, *39*(3), 337–360. https://doi.org/10.1177/0309133314567584

Gleason, C., Garambois, P.-A., & Durand, M. (2017). Tracking river flows from space. *Eos*, 98. https://doi.org/10.1029/2017EO078085

Gleason, C. J., & Hamdan, A. N. (2017). Crossing the (watershed) divide: Satellite data and the changing politics of international river basins. *The Geographical Journal*, *183*(1), 2–15. https://doi.org/10.1111/geoj.12155

Gleason, C. J., Wada, Y., & Wang, J. (2018). A hybrid of optical remote sensing and hydrological modeling improves water balance estimation. *Journal of Advances in Modeling Earth Systems*, *10*, 2–17. https://doi.org/10.1002/2017MS000986

Gleason, C. J., & Wang, J. (2015). Theoretical basis for at-many-stations hydraulic geometry. *Geophysical Research Letters*, *42*, 7107–7114. https://doi.org/10.1002/2015GL064935

Gupta, H. V., Kling, H., Yilmaz, K. K., & Martinez, G. F. (2009). Decomposition of the mean squared error and NSE performance criteria: Implications for improving hydrological modelling. *Journal of Hydrology*, *377*(1), 80–91. https://doi.org/10.1016/j.jhydrol.2009.08.003

Hagemann, M. W., Gleason, C. J., & Durand, M. T. (2017). BAM: Bayesian AMHG-Manning inference of discharge using remotely sensed stream width, slope, and height. *Water Resources Research*, *53*, 9692–9707. https://doi.org/10.1002/2017WR021626

Hannah, D. M., Demuth, S., van Lanen, H. A. J., Looser, U., Prudhomme, C., Rees, G., et al. (2011). Large-scale river flow archives: Importance, current status and future needs. *Hydrological Processes*, *25*(7), 1191–1200. https://doi.org/10.1002/hyp.7794

Hunt, B. R., Kostelich, E. J., & Szunyogh, I. (2007). Efficient data assimilation for spatiotemporal chaos: A local ensemble transform Kalman filter. *Physica D*, *230*(1), 112–126. https://doi.org/10.1016/j.physd.2006.11.008

Ichii, K., Ueyama, M., Kondo, M., Saigusa, N., Kim, J., Alberto, M. C., et al. (2017). New data-driven estimation of terrestrial CO_2 fluxes in Asia using a standardized database of eddy covariance measurements, remote sensing data, and support vector regression. *Journal of Geophysical Research: Biogeosciences*, *122*, 767–795. https://doi.org/10.1002/2016JG003640

Johns, C. J., & Mandel, J. (2008). A two-stage ensemble Kalman filter for smooth data assimilation. *Environmental and Ecological Statistics*, *15*(1), 101–110. https://doi.org/10.1007/s10651-007-0033-0

Jung, H. C., Jasinski, M., Kim, J.-W., Shum, C. K., Bates, P., Neal, J., et al. (2012). Calibration of two-dimensional floodplain modeling in the central Atchafalaya Basin Floodway System using SAR interferometry. *Water Resources Research*, *48*, W07511. https://doi.org/10.1029/2012WR011951

Katul, G., Wiberg, P., Albertson, J., & Hornberger, G. (2002). A mixing layer theory for flow resistance in shallow streams. *Water Resources Research*, *38*(11), 1250. https://doi.org/10.1029/2001WR000817

Leopold, L. B., Bagnold, R. A., Wolman, M. G., & Brush, L. M. (1960). Flow resistance in sinuous or irregular channels. In *US Geological Survey*. https://doi.org/10.3133/pp282d

López, R., Barragán, J., & Colomer, M. À. (2007). Flow resistance equations without explicit estimation of the resistance coefficient for coarse-grained rivers. *Journal of Hydrology*, *338*(1), 113–121. https://doi.org/10.1016/j.jhydrol.2007.02.027

Martino, L., Luengo, D., & Miguez, J. (2018). Independent random sampling methods, *Statistics and Computing*. Cham, Switzerland: Springer.

McCabe, M. F., Rodell, M., Alsdorf, D. E., Miralles, D. G., Uijlenhoet, R., Wagner, W., et al. (2017). The future of Earth observation in hydrology. *Hydrology and Earth System Sciences*, *21*(7), 3879–3914. https://doi.org/10.5194/hess-21-3879-2017

Moramarco, T., Barbetta, S., Bjerklie, D. M., Fulton, J. W., & Tarpanelli, A. (2019). River bathymetry estimate and discharge assessment from remote sensing. *Water Resources Research*, *55*, 6692–6711. https://doi.org/10.1029/2018WR024220

Oubanas, H., Gejadze, I., Malaterre, P.-O., Durand, M., Wei, R., Frasson, R. P. M., & Domeneghetti, A. (2018). Discharge estimation in ungauged basins through variational data assimilation: The potential of the SWOT mission. *Water Resources Research*, *54*, 2405–2423. https://doi.org/10.1002/2017WR021735

Oubanas, H., Gejadze, I., Malaterre, P.-O., & Mercier, F. (2018). River discharge estimation from synthetic SWOT-type observations using variational data assimilation and the full Saint-Venant hydraulic model. *Journal of Hydrology*, *559*, 638–647. https://doi.org/10.1016/j.jhydrol.2018.02.004

Paiva, R. C. D., Durand, M. T., & Hossain, F. (2015). Spatiotemporal interpolation of discharge across a river network by using synthetic SWOT satellite data. *Water Resources Research*, *51*, 430–449. https://doi.org/10.1002/2014WR015618

Pavelsky, T. M. (2014). Using width-based rating curves from spatially discontinuous satellite imagery to monitor river discharge. *Hydrological Processes*, *28*(6), 3035–3040. https://doi.org/10.1002/hyp.10157

Pavelsky, T. M., Durand, M. T., Andreadis, K. M., Beighley, R. E., Paiva, R. C. D., Allen, G. H., & Miller, Z. F. (2014). Assessing the potential global extent of SWOT river discharge observations. *Journal of Hydrology*, *519*, 1516–1525. https://doi.org/10.1016/j.jhydrol.2014.08.044

Pollard, D. (2002). *A user's guide to measure theoretic probability*. Cambridge, UK: Cambridge University Press.

Rackauckas, C., & Nie, Q. (2017). DifferentialEquations.jl—A performant and feature-rich ecosystem for solving differential equations in Julia. *Journal of Open Research Software*, *5*(1), 15. https://doi.org/10.5334/jors.151

Rosgen, D. L. (1994). A classification of natural rivers. *Catena*, *22*(3), 169–199. https://doi.org/10.1016/0341-8162(94)90001-9

Schumm, S. A. (1985). Patterns of alluvial rivers. *Annual Review of Earth and Planetary*, *13*(1), 5–27.

Smith, L. C., & Pavelsky, T. M. (2008). Estimation of river discharge, propagation speed, and hydraulic geometry from space: Lena River, Siberia. *Water Resources Research*, *44*, W03427. https://doi.org/10.1029/2007WR006133

Sugiura, N., Masuda, S., Fujii, Y., Kamachi, M., Ishikawa, Y., & Awaji, T. (2013). A framework for interpreting regularized state estimation. *Monthly Weather Review*, *142*(1), 386–400. https://doi.org/10.1175/MWR-D-12-00231.1

Tarpanelli, A., Brocca, L., Lacava, T., Melone, F., Moramarco, T., Faruolo, M., et al. (2013). Toward the estimation of river discharge variations using MODIS data in ungauged basins. *Remote Sensing Environment*, *136*, 47–55. https://doi.org/10.1016/j.rse.2013.04.010

Tuozzolo, S., Lind, G., Overstreet, B., Mangano, J., Fonstad, M., Hagemann, M., et al. (2019). Estimating river discharge with swath altimetry: A proof of concept using AirSWOT observations. *Geophysical Research Letters*, *46*, 1459–1466. https://doi.org/10.1029/2018GL080771

Vrugt, J. A., & Beven, K. J. (2018). Embracing equifinality with efficiency: Limits of acceptability sampling using the DREAM (LOA) algorithm. *Journal of Hydrology*, *559*, 954–971. https://doi.org/10.1016/j.jhydrol.2018.02.026

Wang, W.-J., Peng, W.-Q., Huai, W.-X., Katul, G. G., Liu, X.-B., Qu, X.-D., & Dong, F. (2019). Friction factor for turbulent open channel flow covered by vegetation. *Scientific Report*, *9*(1), 1–16. https://doi.org/10.1038/s41598-019-41477-7

Yoon, Y., Durand, M., Merry, C. J., Clark, E. A., Andreadis, K. M., & Alsdorf, D. E. (2012). Estimating river bathymetry from data assimilation of synthetic SWOT measurements. *Journal of Hydrology*, *464-465*, 363–375. https://doi.org/10.1016/j.jhydrol.2012.07.028

Zhu, D., Chen, Y., Wang, Z., & Liu, Z. (2011). Simple, robust, and efficient algorithm for gradually varied subcritical flow simulation in general channel network. *Journal of Hydraulic Engineering*, *137*(7), 766–774. https://doi.org/10.1061/(asce)hy.1943-7900.0000356